Electronic structure and defect properties of B_6O from hybrid functional and many-body perturbation theory calculations: A possible ambipolar transparent conductor

J. B. Varley and V. Lordi
Lawrence Livermore National Laboratory, Livermore, California, 94550, USA

A. Miglio and G. Hautier
Institut de la matière condensée et des nanosciences (IMCN), European Theoretical Spectroscopy Facility (ETSF), Université Catholique de Louvain, Chemin des étoiles 8, bte L7.03.01, 1348 Louvain-la-Neuve, Belgium

(Received 3 May 2014; revised manuscript received 27 June 2014; published 16 July 2014)

B_6O is a member of icosahedral boron-rich solids known for their physical hardness and stability under irradiation bombardment, but it has also recently emerged as a promising high mobility p-type transparent conducting oxide. Using a combination of hybrid functional and many-body perturbation theory calculations, we report on the electronic structure and defect properties of this material. Our calculations identify B_6O has a direct band gap in excess of 3.0 eV and possesses largely isotropic and low effective masses for both holes and electrons. Of the native defects, we identify no intrinsic origin to the reported p-type conductivity and confirm that p-type doping is not prevented by intrinsic defects such as oxygen vacancies, which we find act exclusively as neutral defects rather than hole-killing donors. We also investigate a number of common impurities and plausible dopants, finding that isolated acceptor candidates tend to yield deep states within the band gap or act instead as donors, and cannot account for p-type conductivity. Our calculations identify the only shallow acceptor candidate to be a complex consisting of interstitial H bonded to C substituting on the O site $(CH)_O$. We therefore attribute the origins of p-type conductivity to these complexes formed during growth or more likely via isolated C_O which later binds with H within the crystal. Lastly, we identify Si as a plausible n-type dopant, as it favorably acts as a shallow donor and does not suffer from self-compensation as may the C-related defects. Thus, in addition to the observed p-type conductivity, B_6O exhibits promise of n-type dopability if the stoichiometry and both native and extrinsic sources of compensation can be sufficiently controlled.

DOI: 10.1103/PhysRevB.90.045205 PACS number(s): 61.72.Bb, 61.72.J−, 71.20.−b, 71.55.Ht

I. INTRODUCTION

Many technologies require high electrical conductivity combined with good carrier mobility and transparency in the visible range [1], all of which are properties satisfied by transparent conducting oxides (TCOs) [2,3]. While n-type TCOs are ubiquitous in modern technology, their p-type counterparts lag behind due to limitations in doping and significantly lower carrier mobilities, often by at least an order of magnitude [4,5]. Recent computational efforts have attempted to bridge this gap by performing a high-throughput screening study to identify oxide candidates that combine a large band gap (for optical transparency) and a low hole effective mass (for high hole mobility) [6], two fundamental criteria for a desirable p-type TCO. One of the compounds identified through this study is B_6O or boron suboxide. The screening found that this compound exhibits a low hole effective mass (around 0.6 compared to >2 for current Cu-based p-type TCOs such $CuAlO_2$ [7], $CuCrO_2$ [8], or $SrCu_2O_2$[9]) and a large band gap (3 eV according to G_0W_0 computations). Boron suboxide has mainly been studied as a hard coating material [10,11] and we are aware of only one paper that measured its transport properties [12]. While Akashi *et al.* concluded that B_6O can be p-type as-grown, their samples were largely porous and may not accurately reflect the fundamental bulk properties [12].

Here we use a combination of G_0W_0 and hybrid functional calculations to study the electronic structure of B_6O and its defect thermodynamics. We first discuss the band structure of B_6O as calculated with both methods, confirming that this material meets several criteria for a p-type TCO. We then compute defect formation energies with the hybrid functional, investigating the electronic and structural properties of native defects and a number of impurity and dopant atoms to assess the dopability of this material. We find that no native defects can account for the reported p-type behavior, with the most favorable acceptor B_O acting as a deep rather than shallow acceptor. We also find no evidence that native defects would compensate p-type material, with oxygen vacancies (V_O) only stable as neutral defects and B_i donors high in energy. Furthermore, we find that hole small polarons are not stable in this material, and that reports of polaronic hole transport are likely a result of defective material rather than an intrinsic property.

In terms of impurities, our results suggest that typical doping schemes do not apply to B_6O due to the unique bonding environment exhibited by the underlying icosahedral structure [13,14], with the majority of substitutional and interstitial impurities acting as deep donors or acceptors. However, we do identify a complex consisting of H and C substituting on the oxygen site that acts as a shallow acceptor and is likely responsible for the observed p-type conductivity in this oxide semiconductor [12]. Our results confirm B_6O to be a plausible candidate for a p-type TCO and additionally show implications for ambipolar doping if the stoichiometry and background impurity concentration can be controlled.

II. COMPUTATIONAL DETAILS

The calculations employing many-body perturbation theory in the GW framework have been performed using the ABINIT code and norm-conserving pseudopotentials [16]. The

 ©2014 American Physical Society

TABLE I. The hexagonal lattice constants, bulk modulus (B_0), formation enthalpy (ΔH_f), and direct band gap of B_6O, calculated using DFT with the HSE functional and within the G_0W_0 approximation. Available experimental values from Refs. [11] and [15] are listed for comparison.

	a (Å)	c (Å)	B_0 (GPa)	ΔH_f (eV)	E_g (eV)
G_0W_0 : GGA	5.393	12.318	–	–	3.00
HSE (32%)	5.353	12.255	246	−5.29	3.11
Expt.	5.399[a]	12.306[a]	181[a]	–	–
	5.312[b]	12.361[b]	181–314[b]	–	–

[a]Reference [11].
[b]Reference [15].

single-shot G_0W_0 approach was performed using wave functions generated from density functional theory (DFT) with the generalized gradient approximation (GGA). All hybrid functional calculations have been carried out using the VASP code [17] with the screened hybrid functional of Heyd, Scuseria, and Ernzerhof (HSE06) [18] within the projector augmented wave (PAW) approach [19]. Since the experimental band gap of B_6O is not known to our knowledge, the Hartree-Fock mixing parameter was set to 32% to more closely reflect the band gap as calculated within the G_0W_0 approximation. The resulting bulk properties are summarized in Table I and also agree well with available experimental values. We adopt the hybrid functional for all defect calculations to improve the description of localized defect states and overcome limitations arising from the underestimation of the band gap as calculated using DFT with functionals like the LDA and GGA (see Table I) [20].

The effective masses have been computed by performing an interpolation with Boltztrap [21] on a GGA uniform grid band structure obtained from the Materials Project [21,22]. We use an average effective mass defined as [6]

$$\bar{\mathbf{M}}_{\alpha\beta}^{-1} = \frac{-\sum_i \int \left[\frac{1}{\hbar^2}\frac{\partial^2}{\partial k_\alpha \partial k_\beta} E(i,\mathbf{k})\right] f[E(i,\mathbf{k}),\epsilon_F,T]\frac{d\mathbf{k}}{4\pi^3}}{\sum_i \int f[E(i,\mathbf{k}),\epsilon_F,T]\frac{d\mathbf{k}}{4\pi^3}}, \quad (1)$$

where $E(i,\mathbf{k})$ is the energy of the ith band at the $\mathbf{k}$ wave vector, and $f(E,\epsilon_F,T)$ is the Fermi-Dirac distribution at an electron chemical potential ϵ_F and temperature T. For electrons, the Fermi level ϵ_F is relative to the conduction band minimum (CBM) $E_g - \epsilon_F$, while for holes it is relative to the valence band maximum (VBM) ϵ_F. Evaluated at a given temperature and carrier concentration, the average tensor $\bar{\mathbf{M}}_{\alpha\beta}$ can be used to compare the intrinsic tendency for materials to lead to mobile charge carriers. In this work we adopt a temperature of $T = 300$ K and an ϵ_F leading to a carrier concentration of 10^{18} cm^{-3} for both the hole and electron effective masses. This approach naturally takes into account nonparabolicity, anistropy and the competitions of pockets in the Brillouin zone.

For the defect calculations, we used a plane-wave basis set with a cutoff of 400 eV, a 168-atom supercell and a 2×2×2 grid of Monkhorst-Pack k points. All defect calculations were spin polarized. Corrections for the Coulomb interaction of charged defects were explicitly included following the scheme described by Freysoldt *et al.* [23,24]. For these corrections we used the weighted spatial average of the static dielectric constant $\bar{\epsilon}_0 = 6.4$ as calculated using density functional perturbation theory within the GGA.

III. RESULTS AND DISCUSSION

A. Bulk properties

The structure of boron suboxide is derived from α-rhombohedral boron (space group $R\bar{3}m$) in which O atoms are inserted between the icosahedral B_{12} units [11,25,26]. The structure is presented in Fig. 1(a), which highlights how the O atoms act as bridges between adjacent B_{12} icosahedra and result in two inequivalent B sites. We label these sites as B_I bonded only to other B_I within the icosahedra and B_{II} that bond to the oxygen and B_I sites. All O atoms are bonded to three B and are symmetrically equivalent.

The lattice parameters of B_6O are known to be highly sensitive to the stoichiometry [11,15], with the experimental values in Table I extrapolated to ideal stoichiometry by Kurakevych *et al.* in agreement within 1% of our calculated values. More recent estimates extracted from the literature by Slack *et al.* are also included in Table I and are in

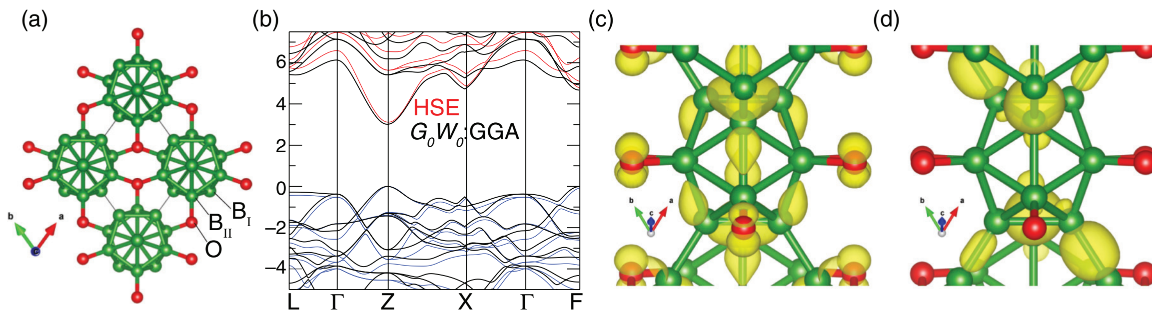

FIG. 1. (Color online) (a) Structure of B_6O that shows the B_{12} icosahedral units bridged by B atoms (B_I-B_I linkages) and threefold coordinated O atoms (O-B_{II} linkages). (b) The band structure along symmetry lines as calculated using HSE (red and blue) and G_0W_0 : GGA (black). For comparison purposes, the G_0W_0 band structure was computed using the relaxed atomic structure determined with HSE. Charge density isosurfaces of the valence band maximum located at (c) the Z point and (d) the Γ point. All isosurfaces are shown at 20% of their maximum value.

TABLE II. Computed electron and hole effective mass within GGA for the two ambipolar candidates SnO and $CuInO_2$ compared to B_6O. The three M_1, M_2, M_3 values are the eigenvalues of the average effective mass tensor at 300 K and a concentration of carriers of 10^{18} cm^{-3}. The B_6O values computed with HSE are also included for comparison. All masses are reported relative to the electron mass m_0.

		m_e^* (m_0)			m_h^* (m_0)		
Material	Space group	M_1	M_2	M_3	M_1	M_2	M_3
SnO	$P4/nmm$	0.26	0.26	0.44	0.66	2.77	2.77
$CuInO_2$	$R\bar{3}m$	0.44	0.44	0.50	1.74	1.74	6.7
B_6O	$R\bar{3}m$	0.31	0.39	0.39	0.42	0.71	0.71
B_6O (HSE)	$R\bar{3}m$	0.3	0.35	0.35	0.34	0.65	0.65

comparable agreement with our results [15]. This sensitivity to stoichiometry also extends to the bulk modulus (B_0), with values reported from 181 to 314 GPa for samples containing various amounts of O deficiency, estimated to be between ~0–40% by Slack *et al.* [15]. Our calculated B_0 of 246 GPa is lower than the 314 GPa reported for stoichiometric B_6O [15], but it still identifies B_6O as an incredibly hard material.

We now turn to the electronic band structure included in Fig. 1(b), which shows that B_6O has a direct gap with the VBM and CBM at the Z point. We find good overall qualitative agreement in the band structure between the HSE and G_0W_0 calculations, but there are differences in the relative band positions away from the band edges that likely result from the strong covalency of B_6O. The very dispersive valence band at Z leads to a low hole effective mass (~0.4–0.7 m_0), which we include in Table II. The agreement between the different methods and previous calculations [6] suggests the large dispersion of the VBM is correctly described and largely insensitive to the choice of functional.

The valence band's wave function at Z is shown in Fig. 1(c) and reveals the VBM has a B p-derived contribution distributed around the faces of the icosahedra and an O p_z character roughly perpendicular to the O-B_{II} bonding plane. In contrast to the disperse VBM at Z, the valence band at Γ is much flatter and indicates heavier holes. Consistent with this interpretation, the character of the wave function at Γ [Fig. 1(d)] is found to be more localized on the covalent bonds between B_I atoms that link isolated icosahedra. Thus holes delocalize on the icosahedra with transport expected to be dominated along the linkages of O-B_{II} rather than B_I-B_I.

While B_6O was identified as a prospective p-type TCO for its low hole effective mass [6], we also find that the conduction band shows a large dispersion at the Z point. The character of the wave function at the CBM at Z is similar to the VBM [Fig. 1(c)] in that it has contributions both from B states distributed within and around the icosahedra (B s and p) and from the bridging O atoms (of predominantly O s character). Compared to the hole effective mass, the calculated electron effective mass tensor is lower and even more isotropic (between 0.31 and 0.39 m_0) and only about twice that of the best known n-type TCOs [27]. The combined low effective masses of both carrier types make this material a candidate for a high mobility ambipolar TCO if n-type doping can be achieved. The two TCOs that have shown ambipolar doping behavior such as $CuInO_2$ [28,29] and SnO [30–32] both have larger and more anisotropic hole effective masses (see Table II), suggesting B_6O could be a more promising alternative.

The band structure of B_6O had already been studied within DFT [33,34], where the reported values for the band gap are in the same order than our GGA results (from 2 to 2.4 eV) and significantly smaller than the results we obtain using HSE and G_0W_0 (Table I). This large underestimation of DFT is known and expected. As far as we know, no experimental measurement of the material's band gap has been reported in the literature. Claims of a band gap of 2 eV based on the DFT results and the red color of certain B_6O crystals have been reported [25], as well an estimate of 2.50 eV based on extrapolated values for stoichiometric B_6O [15]. Considering the G_0W_0 results, which tend to slightly underestimate the experimental band gap [35], such a small band gap is unlikely and the red color of the crystals is more likely a result of defects. Supporting that the 2 eV absorption is not a fundamental property of the electronic structure, the color of samples have been reported to vary dramatically depending on synthesis conditions from brown to red-orange [25] to colorless for some crystals [36].

B. Defect properties

To clarify the role of defects in B_6O, we calculate defect formation energies (E^f), from which we can derive equilibrium concentrations and address the stability of different charge states and the related electronic transition levels [37]. The defect formation energy is given by

$$E^f[D^q] = E_{\text{tot}}[D^q] - E_{\text{tot}}[\text{bulk}] + \sum_i n_i(E_i + \mu_i) + q(\epsilon_F - \epsilon_{\text{VBM}}) + \Delta^q, \quad (2)$$

where $E_{\text{tot}}[D^q]$ and $E_{\text{tot}}[\text{bulk}]$ represent the total energy of the supercell containing a defect D in charge state q, and that of a perfect host crystal in the same supercell. The elemental reference energies E_i are calculated from the energy per atom of the standard state at $T = 0$ K for each species added or removed from the supercell, i.e., α-B, C, Si, O_2(g), H_2(g), and N_2(g). Contributions due to the high temperatures and pressures typical of B_6O growth can be taken from thermodynamic tables [38].

Additional contributions to the chemical potentials (μ_i) vary depending on the experimental conditions during growth or annealing, which can range from B-poor (O-rich) to B-rich (O-poor). The B-rich limit is taken with respect to α-B ($\mu_B = 0$, $\mu_O = \Delta H[B_6O]$), while the O-rich limit is given by the equilibrium condition between B_6O and B_2O_3 ($\mu_B = \frac{\Delta H[B_2O_3] - 3\Delta H[B_6O]}{16}$), for which we calculate a formation enthalpy of $\Delta H[B_2O_3] = -12.71$ eV. The chemical potential limits have been obtained for any extrinsic defect ($X =$ H, N, C, Si) by identifying competitive phases in the X-B-O-H phase diagram using the Materials Project database [39]. The competitive phases include B_9H_{11}, BN, $B_6H_{10}N$, NH_3, $B_{13}C_2$, $B_9H_{11}C_2$, $H_{34}C_{19}$, and α-SiO_2, with all reference energies computed consistently with the HSE functional at $T = 0$ K (see Appendix A). From these energies, we used the pymatgen

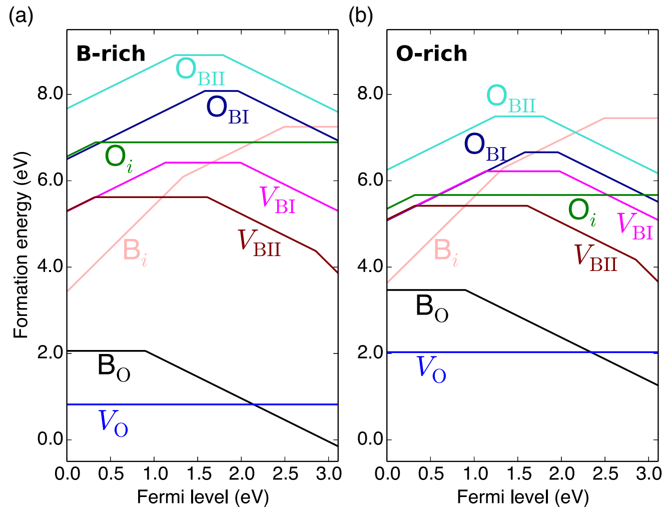

FIG. 2. (Color online) Defect formation energy vs Fermi level for intrinsic defects in B_6O for (a) boron-rich and (b) oxygen-rich conditions as defined in the text. The Fermi level is referenced to zero at the VBM. Defects on the O site are always more favorable than interstitials and native defects on the B sites.

package to obtain the chemical potential associated with the lowest extrinsic defect formation energy in either O-rich or O-poor conditions [22]. The ϵ_F is referenced to the VBM of the host ($\epsilon_{\rm VBM}$) and ranges over the band gap. Finally, the Δ^q term represents the Freysoldt correction that accounts for the image-charge correction for charged impurities and the proper alignment of the electrostatic potential between the pristine and defective supercells [23,24]. We note that our choice for the chemical potentials only affects the absolute formation energies and does not affect the charge state transition levels.

In Fig. 2 we plot the formation energies of the energetically most favorable native defects for B-rich to O-rich conditions. We considered $V_{\rm O}$, the B vacancies ($V_{\rm BI}$, $V_{\rm BII}$), B and O interstitials (B_i, O_i), and antisite defects of O substituted on the B sites ($O_{\rm BI}$, $O_{\rm BII}$) and the B substituted on the O site ($B_{\rm O}$). Figure 2 shows the high energetic cost of disrupting the bonding of the B_{12} icosahedra, which is most apparent from the large formation energies of the $V_{\rm B}$ and $O_{\rm B}$ defects. We find these defects to be amphoteric, acting as compensating deep donors for Fermi levels corresponding to p-type conditions and deep acceptors for n-type conditions. This is in contrast to other p-type TCOs with cation vacancies that behave as shallow acceptors like SnO [31] and Cu_2O [40]. Considering their electrical behavior, the $V_{\rm B}$ and $O_{\rm B}$ cannot account for the reports of p-type conductivity in B_6O. The interstitials, which most favorably bind to individual faces of the B_{12} icosahedra, are deep donors also generally high in energy and will not lead to p-type material either.

Defects associated with the O site are far more favorable, with $V_{\rm O}$ a neutral defect for all Fermi level values within the band gap and $B_{\rm O}$ the most favorable acceptor. The low defect formation energies of the $V_{\rm O}^0$ and $B_{\rm O}$ are in agreement with the tendency for oxygen deficiency experimentally observed in B_6O. The exact stoichiometry of boron suboxide samples is usually noted B_6O_x with x varying from 0.72 to 0.95 depending on the synthesis [25]. Combined with high growth temperatures ranging from ∼1000 to above 2000 °C [12,15,25,41], this complicates the growth of stoichiometric B_6O.

To achieve reliable p-type conductivity, a material needs to possess a suitable concentration of shallow acceptors without suffering from compensation from hole-killing donor defects. For the former, we find the most favorable native acceptor is $B_{\rm O}$, which possesses a deep $\epsilon(0/-)$ charge state transition level 900 meV above the VBM. This ionization energy is much too large to yield any appreciable concentration of ionized holes and cannot explain the hole concentrations of 10^{17} to 10^{19} cm^{-3} measured by Akashi *et al.* [12]. Interestingly, for the latter we find $V_{\rm O}$ remains neutral even in p-type conditions and does not present itself as a barrier to achieving significant hole concentrations. This is a consequence of the distinct bonding environment in B_6O; the creation of a (neutral) $V_{\rm O}$ leaves three electrons from the neighboring B bonds, one which is donated to the icosahedra and two which form a singlet pair [13,14]. Inspection of the atom-projected density of states reveals that this singlet pair is far below the VBM, and that there are no localized states introduced into the band gap which can yield other charge states. Such a property is uncommon for many oxides in which $V_{\rm O}^{2+}$ act as hole-compensating donors for Fermi levels near the VBM [42–44].

While the analysis of intrinsic defects indicates no reason to exclude the possibility of p-type B_6O, there is no shallow intrinsic acceptor explaining an as-grown p-type behavior. Due to the extremely high temperatures and various methods used to synthesize B_6O [12,25,41], we also considered the role of unintentionally incorporated impurities such as H, C, N, and Si. We include the formation energies of the impurities in Fig. 3 for both B-rich and O-rich conditions.

As an isolated interstitial, H_i is stable as a shallow donor for Fermi levels within the band gap and most favorably binds to two $B_{\rm I}$, shared between adjacent B_{12} icosahedra similar to its behavior in α-B [45]. Interestingly, H_i^+ bonded to an O site is 0.4 eV higher in energy than when bonded to B, again highlighting the differences in the underlying bonding and electronic structure of B_6O as compared to more conventional semiconducting oxides [46]. Since we find that H_i acts exclusively as a donor, we also consider its complexes formed with negatively charged acceptors, which have been shown to enhance the solubility of acceptors in a number of materials [46,47]. H_i may also form complexes post-growth, as its migration barrier is likely similar to the ∼1 eV calculated for H_i^+ in α-B and suggests mobility near room temperature [45]. In Figs. 3(a) and 3(b) we find that complexes formed between H and vacancies (denoted $H_{\rm B}$ and $H_{\rm O}$) are amphoteric defects that only lead to deep states within the band gap. $H_{\rm O}$ is found to come off site and bond to a single $B_{\rm II}$, while the $H_{\rm B}$ species also preferentially bond to adjacent $B_{\rm I}$ rather than O. None of the H_i-vacancy complexes can explain the observed p-type conductivity [12].

H can also favorably interact with the native antisite acceptor $B_{\rm O}^-$ to form a $(BH)_{\rm O}$ complex. We find the formation of the complex electrically passivates the isolated $B_{\rm O}$ for a larger range of Fermi levels, up to the $\epsilon(0/-)$ 2.67 eV above the VBM, but it also stabilizes additional deep acceptor states. Therefore, the $(BH)_{\rm O}$ and $H_{\rm O}$ are the most favorable native acceptor complexes with H, but are still far too deep to account

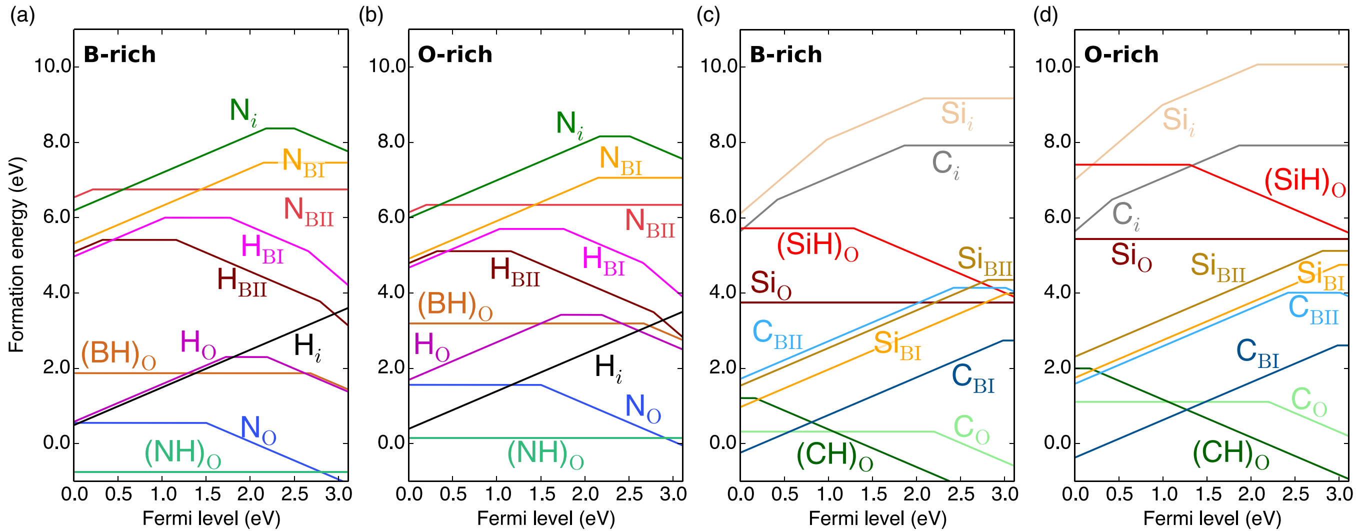

FIG. 3. (Color online) Defect formation energies vs Fermi level for various impurities in B_6O. H and N-related defects are included in the first two panels for B-rich (a) and O-rich (b) conditions, while C and Si-related defects are shown in the last two for B-rich (c) and O-rich (d) conditions. Complexes with H are also shown, with the $(CH)_O$ complex on the O site found to be the only shallow acceptor candidate in B_6O.

for *p*-type conductivity. Defining the binding energy (E_b) as the difference in formation energies of the isolated constituents and the complex, we find the $(BH)_O^0$ complex is more stable than H_i^+ and B_O^- by 1.58 eV. Similarly, the H_O^- acceptor is more stable than the H_i^- and V_O^0 by 3.33 eV. The low formation energy and strong binding energy of H_O therefore represents another challenge for obtaining stoichiometric B_6O.

We also include N impurities in Figs. 3(a) and 3(b), where we find N is always most favorable as a substitutional defect on the O site. While the calculated formation energies are low and suggest N_O can be easily incorporated into B_6O, N_O is a deep acceptor with an $\epsilon(0/-)$ 1.51 eV above the VBM and cannot account for the observed *p*-type behavior. We find that N_O also forms a strong neutral $(NH)_O^0$ complex with H_i ($E_b =$ 3.30 eV), suggesting H can effectively passivate the deep states associated with isolated N_O acceptors. Furthermore, the formation energies of the $(NH)_O^0$ complexes appear prohibitively low in the more B-rich limit [Fig. 3(a)], which indicates an instability of B_6O grown in an environment rich in N and H for certain conditions. We remind the reader that all formation energies are reported in the limit of $T = 0$ K, and that the entropic contributions to the gas-phase reference energies in the lower limit of reported B_6O growth temperatures (1365 K) [15,48] would increase the formation energies of the $(NH)_O$ complexes by 1 eV [38]. Regardless, the low formation energies of the N-related impurities raise possible concerns with the suggested use of pyrolytic BN crucibles and an N_2 overpressure in the growth of stoichiometric B_6O crystals [15].

In Figs. 3(c) and 3(d) we show C and Si-related defects and their complexes with H_i. Carbon substitutional impurities are found to be low in energy, most favorably incorporating as a deep acceptor on the O site or as a shallow donor on the B_I site depending on the conditions. This behavior suggests C impurities will self-compensate, acting as either donors (C_{BI}) or acceptors (C_O) depending on whether the Fermi level falls closer to *p*- or *n*-type conditions. The low formation energies of C_{BI} would push the Fermi level away from the VBM, inhibiting *p*-type conductivity in B_6O, until the C_O becomes the energetically preferred configuration. From Figs. 3(c) and 3(d) it can be seen this occurs ∼0.5–1.5 eV above the VBM depending on the conditions, suggesting that isolated C impurities would likely lead to higher Fermi levels not compatible with *p*-type material.

Most significantly, we find C_O can strongly interact with H_i and form a $(CH)_O$ complex that also behaves as an acceptor. Like the isolated C_O, this acceptor complex is low in energy and presumed to form either during growth or post-growth as H_i likely present within the lattice can diffuse and interact with isolated C_O. The $\epsilon(0/-)$ of the $(CH)_O$ is only 170 meV above the VBM, much lower than the $\epsilon(0/-)$ (2.20 eV) or $\epsilon(-/-2)$ (above the CBM) for the isolated C_O, and represents the only identified ionization energy compatible with observed hole concentrations and *p*-type conductivity in B_6O [12]. This behavior of the $(CH)_O$ complex can be understood from the hybridization of the H_i and C_O defect states. C_O^0 contributes four electrons, donating three to satisfy the bonds with neighboring B and one to satisfy the electron deficiency of the icosahedra [13], while the remaining lone-pair state is unoccupied and results in a deep level within the band gap. When the complex is formed, the H 1*s* orbital strongly hybridizes with the C_O states and lowers the energy of the lone pair such that it becomes resonant with the valence band. For the neutral complex this bonding state is only partially filled, so it binds an electron from the higher-lying B_6O valence band states and leaves behind a hole in the VBM, characteristic of a true shallow acceptor. We also attribute the decrease in the ionization energy to the conversion of an sp^2 to sp^3 bonding environment of the C_O. This interpretation is supported by the change in bond angles from $\sim 97^\circ$ to a more tetrahedral-like $\sim 105^\circ$ [13].

Considering the dielectric constant of 6.4ϵ and the hole effective masses (see Table II), the estimated hydrogenic binding energy of the hole is ∼0.1–0.2 eV, compatible with the calculated ionization energy of $(CH)_O$. We find that despite

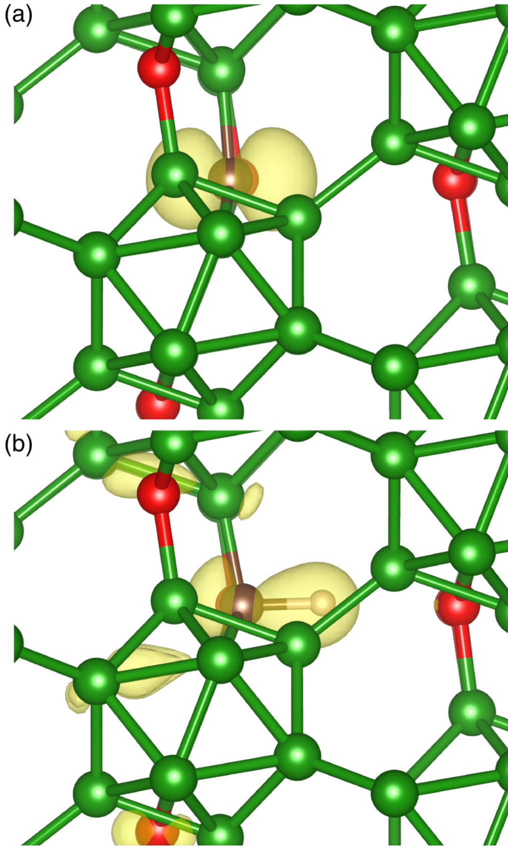

FIG. 4. (Color online) Structure of the isolated C_O^0 defect in B_6O shown in (a) and its complex with H_i, $(CH)_O^0$, shown in (b). The charge density isosurfaces associated with the hole state are included to show the significant hole localization on the C_O^0 in (a) and the $(CH)_O^0$ in (b). The isosurfaces are set at 15% of their maximum value.

such a seemingly shallow level, there is significant hole localization on the $(CH)_O^0$, contrary to the delocalization in the valence band states [e.g., Fig. 1(c)] that would be expected for a true shallow acceptor. This localization is illustrated in Fig. 4, which depicts the charge density isosurfaces of holes localized on the isolated C_O^0 and its complex with H, $(CH)_O^0$. This suggests $(CH)_O^0$ exhibits traits of a deep acceptor but possesses a $\epsilon(0/-)$ close to the VBM, similar to other "shallow" acceptors like the best p-type dopant in GaN, Mg_{Ga} [49].

To assess the stability of the $(CH)_O$, we consider its binding energy with respect to C_O and H_i isolated constituents. In p-type conditions, C_O^0 and H_i^+ are the energetically preferred configurations, with the electron from the H_i donated to the CBM. When the $(CH)_O$ complex is formed, the electron from the H_i is instead contributed to the bonding state, making H_i^0 the most relevant reference and not H_i^+. With respect to the C_O^0 and H_i^0 references, the E_b of $(CH)_O^0$ is 3.03 eV and represents a comparably strong complex relative to H_O and $(NH)_O^0$, and stronger than $(BH)_O^0$. However, if we instead consider the formation energies of H_i^+ and C_O^0 in Fig. 3 for p-type conditions, the $(CH)_O^0$ is predicted to be unstable with an E_b $\sim$−0.5 eV and only becomes stable for Fermi levels >0.24 eV above the VBM. The complex may be kinetically stabilized despite its unfavorable E_b for highly p-type B_6O, since the dissociation of the $(CH)_O$ is still limited by the migration barrier for H_i^+ diffusion [45]. Considering these issues, the long-term stability of p-type conductivity in B_6O warrants further investigation.

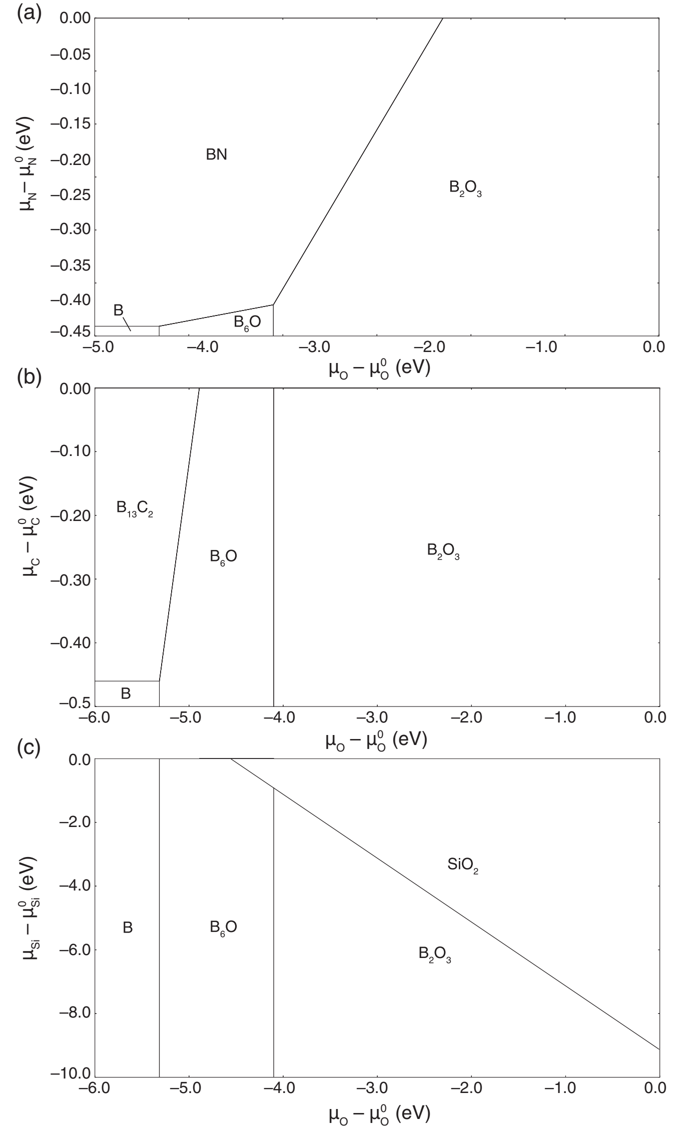

FIG. 5. The X-B-O phase diagrams shown as a function of the oxygen chemical potential (μ_O) versus (a) μ_N for X = N, (b) μ_C for X = C, and (c) μ_{Si} for X = Si. The highest μ_O that ensures the stability of B_6O represents the O-rich limit, while the lowest value represents the B-rich limit.

Incorporated on the B_I site, both C and Si act as shallow donors with ionization energies $\sim$100 meV below the CBM. These ionization energies are also compatible with the $\sim$0.1 eV estimated hydrogenic binding energies of shallow donors in B_6O (see Table II). On the higher energy B_{II} site they act as deep donors, with an acceptor state stabilized for the C_{BII}. However, unlike C, the donor configurations of Si (Si_B) can be more readily incorporated than others such as Si_i, Si_O, and the $(SiH)_O$ deep acceptor complex. This highlights a key distinction between Si and C impurities, as isolated C incorporated in B_6O will exhibit self-compensation effects. For the O-rich conditions in Fig. 3(d), Si_{BI} shallow donors are

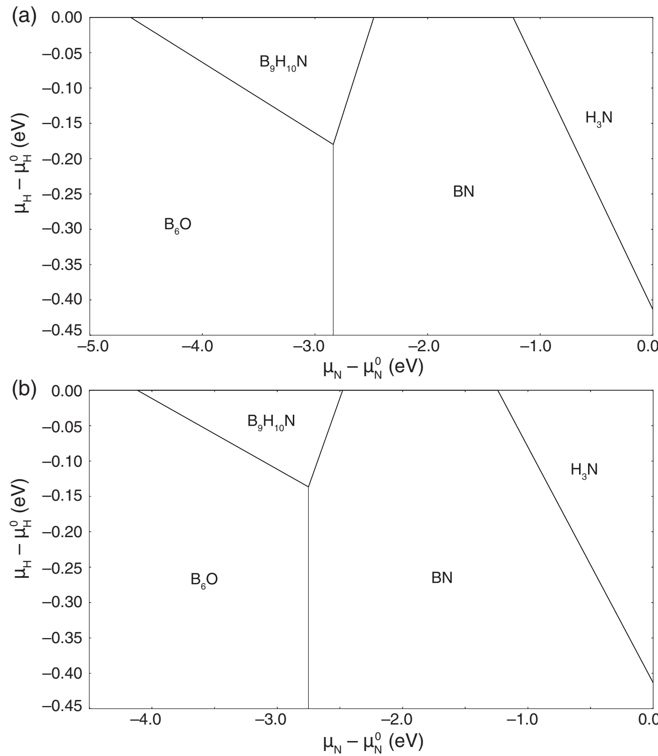

FIG. 6. The N-H-B-O phase diagrams shown for (a) B-rich, reducing conditions and (b) O-rich, oxidizing conditions. The chemical potentials μ_H and μ_N used in Figs. 3(a) and 3(b) were chosen to correspond to their maximum values that simultaneously ensure the stability of B_6O.

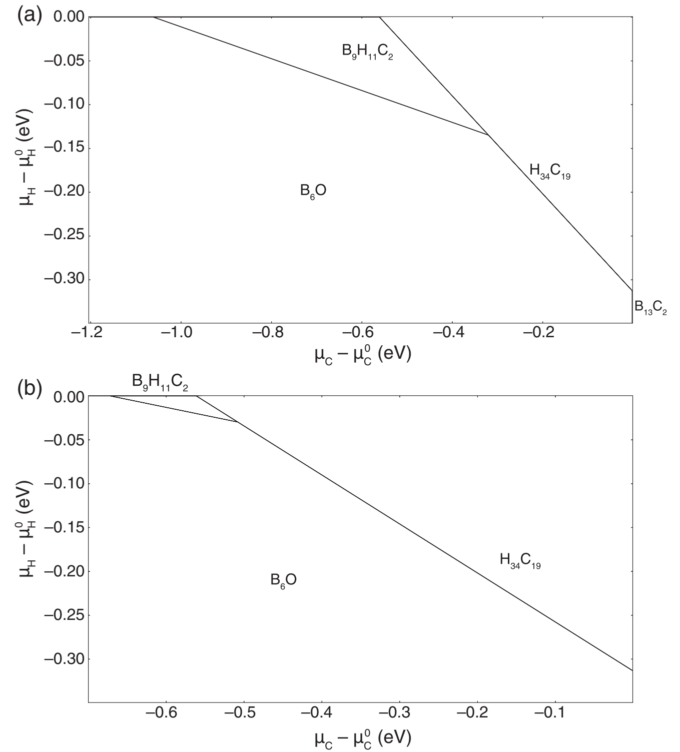

FIG. 7. The C-H-B-O phase diagrams shown for (a) B-rich, reducing conditions and (b) O-rich, oxidizing conditions. The chemical potentials μ_H and μ_C used in Figs. 3(c) and 3(d) were chosen to correspond to their maximum values that simultaneously ensure the stability of B_6O.

the preferred Si defects even in n-type conditions, suggesting Si doping may be a viable route to achieving n-type B_6O if compensation by acceptors can be suppressed. Specifically, this implies limiting the incorporation of C and N impurities during growth and minimizing the formation of native sources of compensation such as B_O^- by growing in the O-rich limit. Using more nonequilibrium growth techniques to incorporate Si may also overcome the narrow range of conditions in which n-type B_6O may be realized.

Lastly, we address the reports by Akashi *et al.* that hole transport in B_6O is mediated by small polarons [12]. This claim must be examined with great caution as many materials, including $CuAlO_2$ [50] and $ZnRh_2O_4$ [51] have been wrongly claimed to be polaronic from transport measurements exhibiting similar activated processes. Moreover, the mobilities measured experimentally (from 0.1 to 1 cm^2/V s) are very high for small polarons according to the Van Daal and Bosman limit [52]. We were unable to stabilize a hole polaron in nondefective bulk B_6O, indicating they are unlikely to form in the stoichiometric material. The measured activated process is likely due to other factors such as grain boundaries, defects, or a large oxygen off-stoichiometry and the resulting disruption of the B_{12} icosahedral bonding network, factors which can be assumed to contribute in the results reported for highly porous p-type B_6O [12]. This is supported by (1) the stability of hole-binding positive charge states of the V_B and O_i native defects for p-type conditions in Fig. 2 and (2) the nature of the hole conduction states in Figs. 1(c) and 1(d). Inspection of the character of states suggests that disorder to the icosahedral bonding network resulting from O deficiency or disorder (see Appendix B) may disrupt fast hole transport [Fig. 1(c)] and enhance much slower hole conduction along B_I-B_I linkages [Fig. 1(d)].

IV. SUMMARY AND CONCLUSIONS

In summary we report on the electronic structure and defect properties of B_6O, a promising high mobility p-type TCO. Of the native defects, we identify no intrinsic origin to the reported p-type conductivity and confirm that p-type doping is not prevented by hole-killing defects such as V_O^{2+}. We consider the role of a number of common impurities and plausible dopant candidates, finding that isolated defects yield deep states within the band gap or act instead as donors, and also cannot account for p-type conductivity. Our calculations identify the only shallow acceptor candidate to be a complex consisting of interstitial H bonded to C_O, a defect that should be present in a substantial concentration due to its low formation energy. In addition, we find that n-type B_6O may also be achievable via Si doping for more O-rich conditions that minimize the simultaneous incorporation of C and formation of other compensating acceptors. Combined with the low hole and electron effective mass, this makes boron suboxide not only a promising p-type TCO but also a possible ambipolar TCO. Controlled synthesis of stoichiometric B_6O is required to

further assess its utility as an electronic material in applications ranging from neutron detectors to transparent electronics.

ACKNOWLEDGMENTS

We gratefully acknowledge useful discussions with T. Ogitsu, X. Gonze, K. E. Morgan, and G. A. Slack. This work was performed under the auspices of the U.S. Department of Energy at Lawrence Livermore National Laboratory under Contract DE-AC52-07NA27344. G.H. acknowledges the F.N.R.S.-FRS as well as the European Union Marie Curie Career Integration (CIG) Grant HTforTCOs PCIG11-GA-2012-321988 for financial support.

APPENDIX A: CHEMICAL POTENTIALS

In Figs. 5–7 we include the calculated phase diagrams generated using the pymatgen package [22]. For the formation energy energies in Figs. 2 and 3 the chemical potentials of each elemental species were chosen to minimize the E^f values while simultaneously ensuring the stability of B_6O from the range of O-rich to B-rich conditions as described in the text. The additional presence of H does not affect the phase diagram for Si as it does for N and C (see Figs. 6 and 7).

APPENDIX B: FRENKEL DISORDER

We can quantify the disorder of the B and O sublattices in B_6O from the reaction energies for Schottky disorder at $T = 0$ by the sum of the defect formation energies in the following reactions:

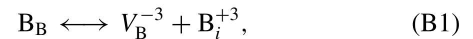

$$\mathrm{B_B} \longleftrightarrow V_{\mathrm{B}}^{-3} + \mathrm{B}_i^{+3}, \quad \text{(B1)}$$

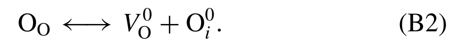

$$\mathrm{O_O} \longleftrightarrow V_{\mathrm{O}}^{0} + \mathrm{O}_i^{0}. \quad \text{(B2)}$$

For the B sublattice, the Frenkel energies range from ∼18 to 20 eV depending on the B site, supporting the high energetic penalty for disrupting the icosahedral bonding network and in line with the observed self-healing ability of irradiated B-rich solids [14,15,53]. For neutral defects in Eq. (B1), the Frenkel energy is ∼13–14 eV. The Frenkel energy for disorder of the O sublattice is 7.8 eV and substantially lower than the disorder energy associated with the B icosahedra, but still high by the standards of conventional semiconductors. Therefore, disorder associated with the O site is expected to dominate due to the formation energy of V_{O}^0 defects, whereas the B icosahedral network is expected to be quite robust to disorder.

[1] K. Ellmer, Nat. Photonics **6**, 809 (2012).
[2] David S. Ginley and C. Bright, MRS Bull. **25**, 15 (2000).
[3] D. S. Ginley, H. Hosono, and D. C. Paine, *Handbook of Transparent Conductors*, 1st ed. (Springer, New York, 2011).
[4] A. Banerjee and K. Chattopadhyay, Prog. Cryst. Growth Charact. Mater. **50**, 52 (2005).
[5] S. Sheng, G. Fang, C. Li, S. Xu, and X. Zhao, Phys. Status Solidi A **203**, 1891 (2006).
[6] G. Hautier, A. Miglio, G. Ceder, G.-M. Rignanese, and X. Gonze, Nat. Commun. **4**, 2292 (2013).
[7] H. Kawazoe, M. Yasukawa, and H. Hyodo, Nature (London) **389**, 939 (1997).
[8] R. Nagarajan, A. D. Draeseke, A. W. Sleight, and J. Tate, J. Appl. Phys. **89**, 8022 (2001).
[9] A. Kudo, H. Yanagi, H. Hosono, and H. Kawazoe, Appl. Phys. Lett. **73**, 220 (1998).
[10] D. He, Y. Zhao, L. Daemen, J. Qian, T. D. Shen, and T. W. Zerda, Appl. Phys. Lett. **81**, 643 (2002).
[11] O. O. Kurakevych and V. L. Solozhenko, J. Superhard Mater. **33**, 421 (2011).
[12] T. Akashi, T. Itoh, I. Gunjishima, H. Masumoto, and T. Goto, Mater. Trans. JIM **43**, 1719 (2002).
[13] D. Emin, J. Solid State Chem. **177**, 1619 (2004).
[14] D. Emin, J. Solid State Chem. **179**, 2791 (2006).
[15] G. A. Slack and K. E. Morgan, J. Phys. Chem. Solids **75**, 1054 (2014).
[16] X. Gonze, B. Amadon, P.-M. Anglade, J.-M. Beuken, F. Bottin, P. Boulanger, F. Bruneval, D. Caliste, R. Caracas, M. Côté, T. Deutsch, L. Genovese, P. Ghosez, M. Giantomassi, S. Goedecker, D. Hamann, P. Hermet, F. Jollet, G. Jomard, S. Leroux, M. Mancini, S. Mazevet, M. Oliveira, G. Onida, Y. Pouillon, T. Rangel, G.-M. Rignanese, D. Sangalli, R. Shaltaf, M. Torrent, M. Verstraete, G. Zerah, and J. Zwanziger, Comput. Phys. Commun. **180**, 2582 (2009).
[17] G. Kresse and J. Furthmuller, Comput. Mater. Sci. **6**, 15 (1996).
[18] J. Heyd, G. E. Scuseria, and M. Ernzerhof, J. Chem. Phys. **118**, 8207 (2003).
[19] P. E. Blöchl, Phys. Rev. B **50**, 17953 (1994).
[20] A. Alkauskas, P. Broqvist, and A. Pasquarello, Phys. Status Solidi B **248**, 775 (2011).
[21] G. K. Madsen and D. J. Singh, Comput. Phys. Commun. **175**, 67 (2006).
[22] S. P. Ong, W. D. Richards, A. Jain, G. Hautier, M. Kocher, S. Cholia, D. Gunter, V. L. Chevrier, K. A. Persson, and G. Ceder, Comput. Mater. Sci. **68**, 314 (2013).
[23] C. Freysoldt, J. Neugebauer, and C. G. Van de Walle, Phys. Rev. Lett. **102**, 016402 (2009).
[24] C. Freysoldt, J. Neugebauer, and C. G. Van de Walle, Phys. Status Solidi B **248**, 1067 (2011).
[25] H. Hubert, B. Devouard, L. A. Garvie, M. O'Keeffe, P. R. Buseck, W. T. Petuskey, and P. F. McMillan, Nature (London) **391**, 376 (1998).
[26] T. Ogitsu, E. Schwegler, and G. Galli, Chem. Rev. **113**, 3425 (2013).
[27] G. Hautier, A. Miglio, D. Waroquiers, G.-M. Rignanese, and X. Gonze (unpublished).
[28] H. Yanagi, T. Hase, S. Ibuki, K. Ueda, and H. Hosono, Appl. Phys. Lett. **78**, 1583 (2001).
[29] M. Sasaki and M. Shimode, J. Phys. Chem. Solids **64**, 1675 (2003).
[30] K. Nomura, T. Kamiya, and H. Hosono, Adv. Mater. **23**, 3431 (2011).
[31] J. B. Varley, A. Schleife, A. Janotti, and C. G. Van de Walle, Appl. Phys. Lett. **103**, 082118 (2013).
[32] N. F. Quackenbush, J. P. Allen, D. O. Scanlon, S. Sallis, J. A. Hewlett, A. S. Nandur, B. Chen, K. E. Smith, C. Weiland, D. A. Fischer, J. C. Woicik, B. E. White, G. W. Watson, and L. F. J. Piper, Chem. Mater. **25**, 3114 (2013).

[33] D. Li and W. Y. Ching, Phys. Rev. B. **54**, 1451 (1996).
[34] S. Lee, S. W. Kim, D. M. Bylander, and L. Kleinman, Phys. Rev. B **44**, 3550 (1991).
[35] M. van Schilfgaarde, T. Kotani, and S. Faleev, Phys. Rev. Lett. **96**, 226402 (2006).
[36] A. Kharlamov and N. Kirillova, Powder Metall. Met. Ceram. **41**, 97 (2002).
[37] C. G. Van de Walle and J. Neugebauer, J. Appl. Phys. **95**, 3851 (2004).
[38] H. Afeefy, J. Liebman, and S. Stein, *Neutral Thermochemical data in NIST Chemistry WebBook, NIST Standard Reference Database Number 69* (National Institute of Standards and Technology, Gaithersburg MD, 2010).
[39] A. Jain, S. P. Ong, G. Hautier, W. Chen, W. D. Richards, S. Dacek, S. Cholia, D. Gunter, D. Skinner, G. Ceder, and K. A. Persson, APL Mater. **1**, 011002 (2013).
[40] D. O. Scanlon, B. J. Morgan, and G. W. Watson, J. Chem. Phys. **131**, 124703 (2009).
[41] M. Herrmann, A. K. Swarnakar, M. Thiele, O. Van der Biest, and I. Sigalas, J. Euro. Ceram. Soc. **31**, 2387 (2011).
[42] A. Zunger, Appl. Phys. Lett. **83**, 57 (2003).
[43] J. Robertson and S. J. Clark, Phys. Rev. B **83**, 075205 (2011).
[44] D. O. Scanlon and G. W. Watson, J. Mater. Chem. **22**, 25236 (2012).
[45] P. Wagner, C. P. Ewels, I. Suarez-Martinez, V. Guiot, S. F. J. Cox, J. S. Lord, and P. R. Briddon, Phys. Rev. B **83**, 024101 (2011).
[46] J. B. Varley, H. Peelaers, A. Janotti, and C. G. Van de Walle, J. Phys.: Condens. Matter **23**, 334212 (2011).
[47] J. Neugebauer and C. G. Van de Walle, Appl. Phys. Lett. **68**, 1829 (1996).
[48] P. M. Bills and D. Lewis, J. Less-Common Met. **45**, 343 (1976).
[49] J. L. Lyons, A. Janotti, and C. G. Van de Walle, Phys. Rev. Lett. **108**, 156403 (2012).
[50] J. Tate, H. L. Ju, J. C. Moon, A. Zakutayev, A. P. Richard, J. Russell, and D. H. McIntyre, Phys. Rev. B **80**, 165206 (2009).
[51] A. R. Nagaraja, N. H. Perry, T. O. Mason, Y. Tang, M. Grayson, T. R. Paudel, S. Lany, and A. Zunger, J. Am. Ceram. Soc. **95**, 269 (2012).
[52] A. Bosman and H. V. Daal, Adv. Phys. **19**, 1 (1970).
[53] M. Carrard, D. Emin, and L. Zuppiroli, Phys. Rev. B **51**, 11270 (1995).